Electrometabolomic Modeling of Microbes: Applications in Fuel Cells and Environment Analysis

Max Fontus [1,*] and Peter Ortoleva[2]

[1]Undergraduate Medical Academy, Prairie View A&M University, Prairie View, TX 77446, USA. [2]Department of Chemistry, Indiana University, Bloomington, IN 47405, USA.

A formalism for simulating coupled metabolic and electrophysiological processes is presented. The resulting chemical kinetic and electrophysiological equations are solved numerically in a manner consistent with the multiscale nature of the problem and implemented as a cell simulator. Metabolic features of this simulator were adapted from *Karyote*, a multi-compartment biochemical cell model. We present the mathematical formalism and its computational implementation as an electrometabolomic cell simulator. Applications to *Geobacter sulfurreducens* in the environment and in a fuel cell are discussed.

*Corresponding author: Max Fontus, Undergraduate Medical Academy, Prairie View A&M University, Prairie View, TX 77446, USA. Phone: 1-936-261-3091, Fax: 1-936-261-3092; E-mail: mafontus@pvamu.edu

Financial Support: This work was funded in part by the Undergraduate Medical Academy at Prairie View A&M University.

Introduction

The coupling of electrophysiological and metabolic processes underlies many cellular phenomena. While there are many cell models that account for biochemistry, membrane potential, membrane transport processes and other cellular processes, there is a need for a simulator that accounts for all these processes and their coupling along with general stoichiometry and transport rate laws. Furthermore, a model is needed that takes into consideration the hierarchical structure of Eukaryotic cells, i.e., compartments within compartments. We begin with a brief overview of cellular metabolomic modeling followed by a presentation of bioelectrochemical modeling, and then present a formalism for electrometabolomic modeling.

Metabolomic Modeling

The metabolome is a network of biochemical reactions where outputs from one reaction are inputs to others**.** Metabolomic modeling started with studies on glycolysis [1-4]. Rate constants in these chemical kinetics models are calibrated with concentrations profile data. This calibration quantifies the interaction of the enzymes with metabolites and cofactors. Since that time there have been many chemical kinetic models for metabolomics [5-9]. In the present context, *Karyote* is a compartmented hierarchical model [10, 11] that forms the basis of the metabolic facet of the present electrometabolomic model. However, *Karyote* does not account for charged species which play pivotal roles in cellular activities. The transport of these charged species affect and are affected by the membrane potential, and since there are many systems where membrane potentials have been measured, the next logical step in the evolution of cell modeling is electrometabolomic modeling, i.e. coupling of metabolomic phenomena with electro-physiological ones.

Importance of Membrane Potentials and Availability of Experimental Data

Membrane potentials are the single most important aspect of electrophysiological modeling**.** Membrane potential is involved in a vast array of metabolic activities from nutrients transport to cell motility and cognitive processes. Electrical potentials are known to play a key role in early development at the single cell stage [12] and even during late development and adult behavior [13]. Thus, in a broad spectrum of processes from development to metabolism, the electrical aspect of cellular behavior must be considered.

Membrane potentials were traditionally measured with electrodes, but NMR has also been used in an indirect approach that has the advantage of being applicable to small cells or intracellular compartments [14, 15]. Another method is to use the distribution of permeant ions, namely radiolabeled ions, to assess the potential across a membrane [16].

Membrane potentials have been measured in such a variety of systems that they may be considered a universal feature of cell behavior. While they are well-known in nerve cells, they have been observed in the following cell types (a list that is meant to be suggestive rather than comprehensive):

- *Trypanosoma brucei* [17]
- Human Atrial Cells [18]
- Human Red Blood Cells [19]
- Glial Cells [20]
- YeastSpheroplasts [21]
- Paramecium Cilia [21]
- *Escherichia coli* Gial Cells [21]
- Neutrophils [22]
- Squid Schwann Cells [23]
- Rat Melanotroph [24]
- Pulmonary Arterial Smooth Muscle Cells [25]
- CNS Myelinated Axons [26]
- Outer Hair Cells [27]
- Mouse Embryonic Ventricular Myocytes [28]
- Rabbit Coronary Arterial Cells [29]

The availability of measured potentials in different biochemical systems provides an opportunity to develop and validate an electro-metabolomic model.

Brief Review of Bioelectrochemical Modeling

Bernstein proposed the first quantitative formulation for the origin of bioelectric potentials in terms of the behavior of electrolytic solutions [30, 31]. The theory was advanced and put on firmer basis by Goldman [32] who solved the Nernst -Planck equation for a biological membrane by assuming a constant electrical field. According to this development, the flux of each ion across a membrane depends only on the permeability, the membrane potential, and the aqueous concentration of that ion on both sides of the membrane. The flux of each ion was taken to be independent of interionic interactions. The Goldman-Hodgkin-Katz, GHK, formula for the membrane potential was derived. This equation does not hold for membranes wherein ion pumps and other transmembrane processes are active.

Hodgkin and Huxley applied these concepts to the study of signal propagation in the squid axon. The Hodgkin-Huxley (H-H) model is a set of non-linear differential equations that approximate the electrical characteristics of excitable cells such as neurons and cardiac myocytes [33,34]. Most bioelectrochemical models are extensions of the H-H model [35].

Electrometabolomic Modeling

More comprehensive modeling of electro-metabolomic phenomena involves several challenges. Even local deviations from charge neutrality cause large Coulomb forces. Thus, only complete biochemical reactions, i.e. those that balance charge, should be used. Many cofactors that are necessary for intracellular enzyme-catalyzed reactions and signaling processes are ions such as $Mg^{2+}$and Ca^{2+}. The transport of these ions across the membrane affects and is affected by the membrane potential, which therefore must be accounted for. Thereby, the electrophysiological processes are coupled to biochemical ones. For example,

passive and active transport of ions across membrane potentials affect pH which mediate many intracellular biochemical reactions.

The model presented here is built on a formalism for simulating coupled electro-physiological-metabolic intracellular processes. Specifically, we use equations to describe chemical kinetic/electrophysiological processes. These equations are implemented as a cell simulator using multiscale numerical techniques. The approach is demonstrated via application to a microbial fuel cell powered by *Geobacter sulfurreducens* feeding on acetate anaerobically, and for microbes in the subsurface using oxidized mineral grains as the electron receptor.

Micron and nanometer scale systems present special requirements for reaction-transport theory due to the interplay of Debye layers with larger scale features. For example, processes along and across the nanoscale Debye layer affect the micron-scale dynamics such as bacterial metabolomics or the exchange of charged molecules with the surroundings and across the interior of the system. The objective of this study is to present a mathematical framework for modeling these important systems that overcome computational difficulties imposed by the billions of atoms involved. Thus, we fill a gap between all-atom and macroscopic theory.

Strong Coulomb forces impose charge neutrality in an electrolyte solution. Thus, in the interior of a cell, charge neutrality is maintained in most regions. The question arises as to the distribution of molecules between the interior of a compartment and a Debye layer located at the surface of membranes defining the compartment. Thus the transmembrane flux must be split into a charge-neutral contribution and one that represents exchange with the Debye layers adjacent to the membranes that divide the system into micron-scale compartments. We address this and related issues via a novel electrochemical reaction-transport formalism. This formalism therefore generates a more comprehensive and self-consistent approach that accounts for the many scales on which the spectrum of processes operate.

Materials and methods

Formalism

Compartmentalized Reaction-Transport Model

The cell is divided into N_c compartments labeled $\alpha = 1, \cdots N_c$. There are molecular species labeled $i = 1, \cdots N$; $c_{i\alpha}$ and [species i]$_\alpha$ denote the concentration and activity of species i in compartment α, respectively. Concentrations and electrical potentials are taken to be spatially uniform within a given compartment (except for a thin boundary layer as discussed below). Conservation of mass implies

$$\Omega_\alpha \frac{dc_{i\alpha}}{dt} = \sum_{\alpha' \neq \alpha}^{N_c} A_{\alpha/\alpha'} \tilde{J}_{i\alpha/\alpha'} + \Omega_\alpha \sum_{k=1}^{N_r} \nu_{ik\alpha} W_{k\alpha} \qquad (1)$$

where

$\tilde{J}_{i\alpha/\alpha'}$ = charge-neutral flux of i from α' to α (see below for further definition)

$A_{\alpha/\alpha'}$ = area of membrane separating α from α'

Ω_α = volume of α

$W_{k\alpha}$ = rate of reaction k in α

$\nu_{ik\alpha}$ = stoichiometric coefficient of species i for reaction k in α.

The rate $W_{k\alpha}$ is taken to be in the form

$$W_{k\alpha} = R_{k\alpha}\left[e^{Y_{k\alpha}/RT} - 1\right] \qquad (2)$$

The reverse rate $R_{k\alpha}$ is taken to be in the mass action form while the affinity $Y_{k\alpha}$ is given by

$$Y_{k\alpha} = \sum_{i=1}^{N} \nu_{ik\alpha} \mu_{i\alpha} \qquad (3)$$

for electrochemical potential $\mu_{i\alpha}$. The electrochemical potentials are written in the form

$$\mu_{i\alpha} = \mu_{i\alpha}^{o} + RT \ln a_{i\alpha} + z_i F V_\alpha \qquad (4)$$

where $\mu_{i\alpha}^{o}$ is the reference chemical potential of species *i* in α .The membrane flux $J_{i\alpha/\alpha'}$ is divided into passive and deviatoric contributions:

$$J_{i\alpha/\alpha'} = h_{i\alpha/\alpha'} E_{i\alpha/\alpha'} + J_{i\alpha/\alpha'}^{act.} \qquad (5)$$

for permeability $h_{i\alpha/\alpha'}$, and equilibrium factor $E_{i\alpha/\alpha'}$ that vanishes with $\mu_{i\alpha} - \mu_{i\alpha'}$; $E_{i\alpha/\alpha'}$ is given by

$$E_{i\alpha/\alpha'} = q_{i\alpha/\alpha'} \left(\frac{[\text{species } i]_\alpha - [\text{species } i]_{\alpha'} e^{q_{i\alpha/\alpha'} L_{\alpha/\alpha'}}}{1 - e^{q_{i\alpha/\alpha'} L_{\alpha/\alpha'}}} \right) \qquad (6)$$

where

$$q_{i\alpha/\alpha'} = \mathrm{F} z_i \left(V_\alpha - V_{\alpha'} \right) \Big/ L_{\alpha/\alpha'} RT \qquad (7)$$

F = Faraday's constant

z_i = Valence of *i*

V_α = Electrical potential in α

$L_{\alpha/\alpha'}$ = Thickness of the membrane separating α and α'

This passive flux law is obtained by solving the Nernst-Planck equation assuming the electrical field is constant within the membrane [36]. The formula for $E_{i\alpha/\alpha'}$ reduces to that used earlier for uncharged molecular species [10]. $J_{i\alpha/\alpha'}^{act.}$ is the contribution to the flux arising from active processes.

Electrophysiological Model

Consider a physical picture wherein a compartment is divided into the interior domain and a thin charged layer along the surface of the surrounding membrane. Within a compartment interior, charge neutrality,

$$\sum_{i=1}^{N} z_i c_{i\alpha} = 0 , \qquad (8)$$

is maintained (as can be shown via an asymptotic analysis of the continuum coupled reaction-transport-Poisson equations [37]). When ions emerge from one side of a membrane, they have one of two destinations: the charged boundary layer or the charge-neutral compartment interior. Recall $J_{i\alpha/\alpha'}$ is the total transmembrane flux of *species i* from α' to α . In vector form $\mathrm{F}\,\underline{z}\,\underline{\tilde{J}}_{\alpha/\alpha'}$ is the electrical flux from α' to α . A modified flux $\tilde{J}_{i\alpha/\alpha'}$ is defined to be the flux of species *i* that is transferred from the interior of α ' to that of α , and therefore does not transfer net charge. With this, the charge-neutral flux is given by

$$\underline{\tilde{J}}_{\alpha/\alpha'} = \underline{J}_{\alpha/\alpha'} - \underline{z}_{mob,\alpha/\alpha'} \frac{\underline{z}_{mob,\alpha/\alpha'} \bullet \underline{J}_{mob,\alpha/\alpha'}}{\underline{z}_{mob,\alpha/\alpha'} \bullet \underline{z}_{mob,\alpha/\alpha'}} \qquad (9)$$

Here $\underline{z}_{mob,\alpha/\alpha'}$ is the vector of valences of the species that can transfer between compartment α' and α . Note that $\underline{z}_{mob,\alpha/\alpha'}$ and $\underline{J}_{\alpha/\alpha'}$ have *N* components such that the components for the species that cannot traverse the $\alpha\alpha'$ membrane are zero. It can be verified that $\underline{z} \bullet \underline{\tilde{J}}_{\alpha/\alpha'} = 0$ (i.e. the current due to the charge-neutral flux of the ionic species able to traverse the $\alpha\alpha'$ membrane is zero). Hence, $\underline{\tilde{J}}_{\alpha/\alpha'}$ is the correct flux to use in the equation for mass conservation (Eqn.1) adding the mass transfer to the interior zone beyond the charged boundary layer. This guarantees that if $\underline{z} \bullet \underline{c}_\alpha = 0$ initially in all compartments then it will remain so always.

Consider the charging of the boundary layers surrounding a membrane. From the above, $\mathrm{F} A_{\alpha/\alpha'} \underline{z} \bullet \underline{J}_{\alpha/\alpha'}$ is the net electrical current into α from α' . If $\sigma_{\alpha/\alpha'}$ is the charge/area on the α side of the $\alpha\alpha'$ membrane, then

$\sigma_{\alpha/\alpha'} = -\sigma_{\alpha'/\alpha}$; this follows because strong Coulomb forces ensure that the oppositely charged layers on either side of the $\alpha\alpha'$ membrane balance (otherwise the boundary charge would redistribute to ensure this balance). With this, conservation of charge implies

$$\sum_{\alpha' \neq \alpha} A_{\alpha/\alpha'} \underline{z} \bullet \underline{J}_{\alpha/\alpha'} = \sum_{\alpha' \neq \alpha} A_{\alpha/\alpha'} \frac{d\sigma_{\alpha/\alpha'}}{dt} \qquad (10)$$

Assuming that capacitance $C_{\alpha/\alpha'}$ relates the membrane potential $V_{\alpha/\alpha'}$ ($V_{\alpha/\alpha'} = V_\alpha - V_{\alpha'}$), yields

$$\mathrm{F} \sum_{\alpha' \neq \alpha} A_{\alpha/\alpha'} \underline{z} \bullet \underline{J}_{\alpha/\alpha'} = \sum_{\alpha' \neq \alpha} A_{\alpha/\alpha'} C_{\alpha/\alpha'} \frac{dV_{\alpha/\alpha'}}{dt} \qquad (11)$$

This constitutes a set of coupled differential equations for the potentials V_α in each compartment. Thus, we arrive at a set of *N*+1 equations for the *N*+1variables in each compartment. The convention that the potential is zero in the medium in which the system is immersed completes the electrophysiological model.

It might be stated that charge-preserving exchanges of ions between the charge boundary layer and the compartments interior could take place. For example, Ca^{2+} could exchange with two Na^+ or a Mg^{2+} and this is not accounted for. However, the boundary layer is only the thickness of the Debye length (a few angstroms) and thereby its contribution to overall mass bookkeeping for a given compartment is not significant. The above partitioning of charge does keep track of the net charge in these layers and thus the membrane potential is properly computed.

Trans-Membrane Process Rates

Macromolecules embedded in membranes play a central role in the functioning of a cell. Some of these macromolecules mediate the pumping of ions across a membrane up a chemical potential gradient. They also may introduce highly nonlinear passive transport laws that imply favored directions for selected molecules (i.e., import or export) for a given internal compartment where they participate in particular reactions. Another group of membrane-bound macromolecules mediate processes wherein reactants on one side of a membrane yield products on the other. An example of such a macromolecule is the enzyme glycerol-3-phosphate oxidase that is embedded in mitochondrial membranes [38]. In summary, selective and nonlinear membrane processes play a central role in creating and maintaining the viability and spatial organization of a cell. It is now shown how these membrane reaction and transport processes are accounted for in the present compartmentalized cell model.

The pumping of ions and other active transport across a membrane illustrates how such processes are accounted for in our transmembrane reaction formulation. Consider a process in a membrane separating compartments α and α' such that for each of the *N* species

$$\sum_{i=1}^{N} \left[\xi_{i\alpha/\alpha'} (\text{species } i \text{ in } \alpha) + \xi\!\!\!\!\square_{i\alpha/\alpha'} (\text{species } i \text{ in } \alpha') \right] = 0. \qquad (12)$$

The stoichiometric coefficients $\xi_{i\alpha/\alpha'}$ and $\xi\!\!\!\!\square_{i\alpha/\alpha'}$ are defined as follows. If $\xi_{i\alpha/\alpha'} > 0$ then $\xi_{i\alpha/\alpha'}$ *i*-type molecules appear in compartment α ; if $\xi_{i\alpha/\alpha'} < 0$ then $\xi_{i\alpha/\alpha'}$ *i*-type molecules are removed from compartment α as a result of this process. The $\xi\!\!\!\!\square_{i\alpha/\alpha'}$ terms are similar except for *i*-type molecules in compartment α' . As an example, consider a proton pump for a membrane separating a mitochondrion from the cytosol:

$$\mathrm{H^+(cyto) + ATP^{4-}(cyto) \rightarrow H^+(mito) + ADP^{3-}(cyto) + P_i^-(cyto)} \qquad (13)$$

where P_i is inorganic phosphate. Thus, we have $\xi_{H^+\,cyto/mito} = -1, \xi_{H^+\,cyto/mito} = 1, \xi_{ATP^{4-}\,cyto/mito} = -1$, $\xi_{ADP^{3-}\,cyto/mito} = \xi_{P_i\,cyto/mito} = 1$. With this, the flux $J_{cyto/mito}$ takes the form

$$J_{cyto/mito} = k[H^+]_{cyto}[ATP^{4-}]_{cyto} \quad (14)$$

for rate coefficient *k.* The process has been assumed to be irreversible and, for simplicity, [ ] implies concentration here. More general process rate laws can also be used, e.g.,

$$J_{\alpha/\alpha'} = k \prod_{\xi_{j\alpha/\alpha'}<0} [species \quad j]_{\alpha}^{-\xi_{j\alpha/\alpha'}} \prod_{\xi_{j\alpha/\alpha'}<0} [species \quad j]_{\alpha'}^{-\xi_{j\alpha/\alpha'}} \quad (15)$$

With this, the system evolves via

$$\Omega_{\alpha} \frac{dc_{i\alpha}}{dt} = A_{\alpha/\alpha'} \left(\xi_{i\alpha/\alpha'} J_{\alpha/\alpha'} \right) + \text{other terms} \quad (16)$$

A common cellular feature is a Na^+/K^+ -exchange pump. For example, consider the process

$$3Na^+(\alpha) + 2K^+(\alpha') + ATP^{4-}(\alpha) \rightarrow 2K^+(\alpha) + 3Na^+(\alpha') + ADP^{3-}(\alpha) + P_i^-(\alpha) \quad (17)$$

In this case, the flux law becomes

$$J_{\alpha/\alpha'} = k[Na^+]_{\alpha}^3 [K^+]_{\alpha'}^2 [ATP^{4-}]_{\alpha} \quad (18)$$

The rate coefficients depend on the number of pump macromolecules per membrane area.

Algorithm and Computational Approach

The governing equations presented above are solved numerically using Fortran codes constructed by the authors [35]. The resulted cell simulator accounts for general reaction stoichiometry, both for the bulk medium and transmembrane processes. The implementation is hierarchical, i.e. compartments within compartments are allowed, and all possible connectivities between compartments are accounted for. The simulator is validated and calibrated using experimental data for the bloodstream form of Trypanosoma brucei, the causative agent of sleeping sickness. An input file must be generated that contains all the biochemical, geometrical, and transport information needed to specialize the simulation for the cellular system of interest. When the reaction network , transport and reaction rate data are known, errors are in the micromolar range. [35]. More detailed descriptions of the simulations along with input and output files are provided elsewhere [35]. Simulation times are characteristic of the specific system being modeled and run times are typically one CPU hour for a 30-hour biological simulation involving hundreds of species and a half-dozen compartments. To address the typically wide separation of time scales, the DVODE stiff solver is used [39- 44].

Results

***Geobacter* in the Environment**

Prokaryotic cells are used in this and the following section to demonstrate electro-metabolomic modeling. Observed phenomena exhibited by such cells include the following:

- Membrane potentials
- Active and passive transmembrane fluxes
- Internal biochemical reactions
- Processes involving reactions and products on both sides of the membrane
- Precipitation of organic particles within the cell for internal substrate storage
- Transfer of electrons from the interior to reduce oxidized minerals in the surroundings

The objective of this section is to demonstrate that the methodology of the previous section integrates all such processes into a self-consistent electrometabolomic model. We illustrate how the interaction of a bacterium with oxidized mineral grains in the surroundings and a source of reduced organic molecules can drive ATP-production and energy storage processes fundamental to the functioning of these cells.

The system is divided into three compartments: surroundings (sur), interior zone (int), and the intermembrane space between the interior zone and the outer membrane of the microbe (ims).

The reactions and the compartments in which they are operating are as follows:

$$CH_3COOH(sur) \rightleftarrows CH_3COO^-(sur) + H^+(sur) \quad (19)$$

$$CH_3COOH(int) \rightleftarrows CH_3COO^-(int) + H^+(int) \quad (20)$$

$$CH_3COOH(sur) \rightleftarrows CH_3COOH(int) \quad (21)$$

$$18CH_3COOH(int) \rightleftarrows 16C_2H_3O(int) + 4CO_2(int) + 12H_2O(int) \quad (22)$$

$$CH_3COO^-(int) + ATP^{4-}(int) + CoA^{4-}(int) + H^+(int) \rightleftarrows CH_3COCoA^{4-}(int) + ADP^{3-}(int) + Pi^-(int) + H_2O(int) \quad (23)$$

$$CH_3COCoA^{4-}(int) + 3NAD^+(int) + Q(ims) + ADP^{3-}(int) + Pi^-(int) + H_2O(int) \rightarrow CoA^{4-}(int) + 3NADH(int) + 3H^+(int) + QH_2(ims) + ATP^{4-}(int) + 2CO_2(int) \quad (24)$$

$$NADH(int) + Q(ims) + 5H^+(int) \rightleftarrows NAD^+(int) + QH_2(ims) + 4H^+(ims) \quad (25)$$

$$ATP^{4-}(int) + H^+(int) \rightarrow ADP^{3-}(int) + Pi^-(int) + 2H^+(ims) \quad (26)$$

$$QH_2(ims) + 2Cyto\text{-}cFerric(ims) + 2H^+(int) \rightarrow Q(ims) + 2Cyto\text{-}cFerrous^-(ims) + 4H^+(ims) \quad (27)$$

$$CO_2(cyt) \rightleftarrows CO_2(sur) \quad (28)$$

$$CO_2(int) + H_2O(int) \rightleftarrows H^+(int) + HCO_3^-(int) \quad (29)$$

$$CO_2(sur) + H_2O(sur) \rightleftarrows H^+(sur) + HCO_3^-(sur) \quad (30)$$

$$FeOOH(sur) + H^+(sur) + Cyto\text{-}cFerrous^-(ims) \rightarrow Cyto\text{-}cFerric(ims) + FeO(sur) + H_2O(sur) \quad (31)$$

Initial data are provided in Tables 3 and 4. The algorithm and computational approach used are described in the *Materials and Methods* Section. Acetate permeability was taken to be unidirectional. A proton pump as described in equation 26 drives the interior negative relative to the surroundings. Total phosphate in the interior was conserved (i.e., the permeability of phosphate-bearing species was taken to be 0). The transport asymmetry and acetate storage is likely a natural evolutionary adaptation in the minimal subsurface survival conditions that favored *Geobacter* [45]. Resulting simulated electrical potentials in the inter membrane space and in the cell interior, relative to the surroundings, are shown in Figure 1. Predicted membrane potentials are within the same order of magnitude as those reported for similar organisms at comparable external pH condition [61]. The initial potential transient occurs on a short timescale because the overall capacitance of the bacterium (i.e., capacitance/surface area times surface area) is small due to the small size of a bacterium. This is short in contrast to the typical response time of a mammalian cell, which is on the millisecond timescale.

Geobacter Fuel Cell: An Electrometabolomic Circuit

The presentation of the electrometabolomic network below is organized by following the current and mass flows around the biofuel cell of Figure 2. A definition of the variables used is in Tables 1 and 2.

Redox Intercompartmental Reaction

The redox process driving the fuel cell is cast as a transcompartmental reaction that is taken to be the summary (stoichiometric) reaction

$$Ac^-(cyt) + 2(H_2O)\ (cyt) \rightarrow 2(CO_2)\ (cyt) + 8e^-(be) + 7H^+(cyt) \quad (32)$$

Implicit in this process (Eqn.32) is the assumption that anodic electron transfer is rapid relative to the rate of the redox process, i.e. the latter is rate limiting. Although there may be situations where the anodic electron transfer is rate limiting, such situations will, for the most part, be contingent upon the degree of polarizability of the cathode used. The current computed as a result of this process can be considered a maximum current that can be generated from the oxidation of acetate.

Electrode-to-Electrode Electron Transfer

This process accounts for the transfer of electrons from the bioelectrode to the reference electrode through the application device, represented by the resistor R of Figure 2, i.e.

$$e^-(be) \rightleftarrows e^-(re) \quad (33)$$

As the electrons reside near the surface of the electrodes, this is a surface-to-surface process

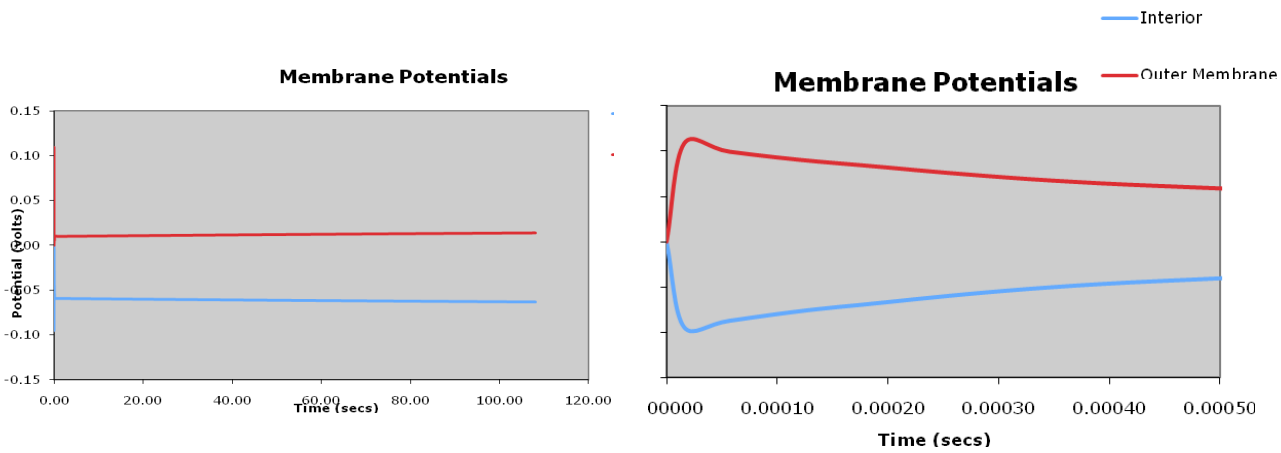

Figure 1. (left) Membrane potentials for the interior and intermembrane space. The interior potential is measured relative to the intermembrane space. The membrane potential of the outer membrane is that of the intermembrane space minus that of the external medium. These values are on the order of magnitude of those observed [61]. (Left) Full time course showing establishment of a steady state, and (Right) expanded plot resolving initial transient that takes place on the 50 microsecond timescale due to the low capacitance of the overall bacterial outer membrane.

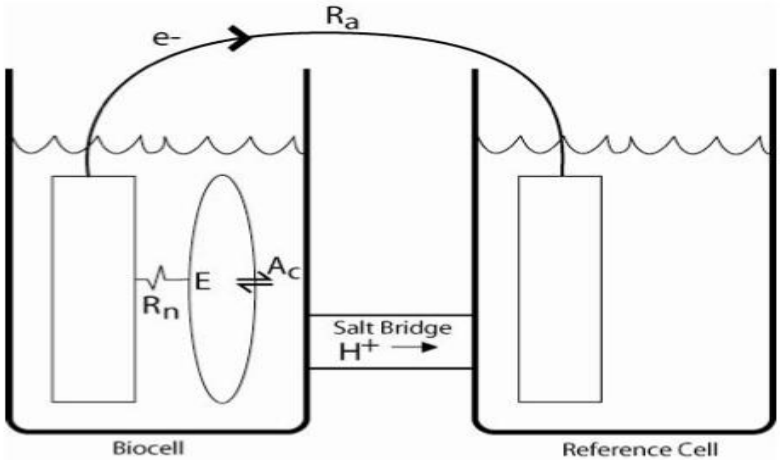

Figure 2. Schematic microbial fuel cell circuit diagram.

Table 1. Definition of Variables

Variable	Definition
V_α	Electrical potential in compartment α
[species i] $_\alpha$	Activity of molecular component i in compartment α
$c_{i\alpha}$	Molar concentration of molecular component i in compartment α
r, R	Resistance of the nanowires and application, respectively (Figure 2)
Ω_α, $A_{\alpha/\alpha'}$	Volume of compartment α, surface area between compartment α and α'
$C_{\alpha/\alpha'}$	Capacitance of membrane separating α and α'
K_ℓ	Equilibrium constant for process ℓ
F	Faraday's constant
β	F/R_gT for gas constant R_g, absolute temperature T.

Table 2. Abbreviations indicate the compartment (spatial zone) in which a variable is relevant.

Abbreviation	Definition
be, bs	Bio-Electrode, Bio-Solution
re, rs	Reference Electrode, Reference Solution
int	Interior zone within a microbe
PEM	Protein Exchange Membrane between the bio- and reference solutions
Ims	Intermembrane space

Table 3. Experimental Values Used In The Calibration Of Parameters Found In Table 4(except for the radius and height for which references are provided). *Geobacter sulfurreducens* morphology was assumed to be cylindrical [60]. Since the current is between the two electrodes, we give the reference electrode a value of zero so that the difference can be the reported value for the 5mM-acetate injection experiment [46]. Assumed total Cation/Anion species represent counterbalancing non-permeating ions.

Species/Current	Biosolution (M)	Bioelectrode (mA)	Reference solution (M)	Reference Electrode (M)
K^+	0.00334	_____	0.00134	_____
Cation	81.66E-03	_____	57.86E-03	_____
Anion	85.000158489E-3	_____	61.200158489E-3	_____
Ac^-	0.005	_____	0.0	_____
H^+	1.58489E-07			1.58489E-07
Current	_____	0.4	_____	0.

Table 4. Calibrated And Literature Parameters Used For *Geobacter sulfurreducens* Physiology. We used the radius and the height to obtain approximated area and volume assuming cylindrical morphology [60]; then we calibrated the area and volume based on the experiment of Bond and Lovley [46]

Parameters	***G. sulfurreducens*** (μm, dm^2, nm^2, mL, S^{-1}, $L^3mmol^{-2}S^{-1}$, $L^5mmol^{-4}S^{-1}$)
Single cell radius	0.5 [65]
Single cell height	0.5 [65]
Total surface area between microbes and biosolution	0.459
Total surface area between microbes and bioelectrode	78.54
Volume of biosolution	19.6345409
Intramicrobial storage reaction	Ac^- Ac*
$K_{storage}$ (rate constant for the storage reaction)	10
$Q_{storage}$ (equilibrium constant for storage reaction)	1000
Transcompartmental Reaction #1	$Ac^-_{cyt} + 2H_2O_{cyt} \rightarrow 2CO_{cyt} + 7H^+_{cyt} + 8e^-_{be}$
Ktrans1 (rate constant for transcompartmental reaction #1)	1.0 EA
Qtrans1 (equilibrium constant for transcompartmental reaction #1)	5.0×10^{14}
Transcompartmental Reaction #2	$2e^-_{re} + 2H^+_{rs} + O_{2,rs} \rightarrow (H_2O_2)_{rs}$
Ktrans2 (rate constant for transcompartmental reaction #2)	1.0 X 10^{-10}
Qtrans2 (equilibrium constant for transcompartmental reaction #2)	1.0 X 10^{35}

(as clarified further below).

Reference Electrode Surface Reaction

Charge is transferred between the reference electrode and the electrolytes via a transcompartmental reaction

$$2e^{-}(re)+2H^{+}(rs)+\left(O_2\right)(rs)\rightleftarrows\left(H_2O_2\right)(rs) \quad (34)$$

As with the redox process within the microbe, we adopt a simplified summary reaction.

Proton Transfer

This circuit element represents the electro-diffusive flux of protons from the bio-solution to the reference solution via the cation exchange membrane separating these two solutions:

$$H^{+}(bs)\rightleftarrows H^{+}(rs) \quad (35)$$

It may be possible for other ions and oxygen to diffuse through the membrane; an undesirable effect of the diffusion of oxygen through the membrane is the decrease in current production of the microbial fuel cell as oxygen can compete with the anode as the final electron acceptor [46]. This effect can be accounted for via the Coulombic efficiency of the fuel cell.

Microbe/Bio-solution Exchange

In the present minimal network, H^+, K^+ and Ac^- are exchanged across the microbial membrane via the passive processes

$$\text{component (bs)}\rightleftarrows\text{component (cyt)} \quad (36)$$

These processes are taken to be driven by electrochemical potential differences.

Bio-electrochemical Reaction-Transport Equations

For component *i* in compartment α, conservation of mass implies

$$\Omega_\alpha\frac{dc_{i\alpha}}{dt}=\sum_{\alpha'\neq\alpha}^{Nc}A_{\alpha/\alpha'}\hat{J}_{i\alpha/\alpha'}+\left(\text{Rxn}\right)_{i\alpha} \quad (37)$$

The last term is the net rate of change in the number of moles of *i* in α due to all reactions in the compartment interior. The surface area separating compartment α from α' is $A_{\alpha/\alpha'}$, $\hat{J}_{i\alpha/\alpha'}$ is the charge neutral flux of component i form α' to α, Ω_α and is the volume of compartment α. Let bracketed quantities be electrochemical activities while $c_{i\alpha}$ is the molar concentration of component i compartment α. With the processes presented above, we have

$$\Omega_{cyt}\frac{d\text{Ac}^-_{cyt}}{dt}=A_{\text{int}/bs}h_{\text{Ac}^-}\left\{\left[\text{Ac}^-\right]_{bs}-\left[\text{Ac}^-\right]_{cyt}\right\}A_{be/\text{int}}W_1 \quad (38)$$

where $A_{\text{be/int}}$ represents the cross-section area of the contact between the nanowire and the redox compartment plus that of any other form of contact transferring electrons between *Geobacter sulfurreducens* and the anode; moreover,

$$W_1=k_1\left[\text{Ac}^-\right]e^{\beta\left(V_{be}-V_{cyt}\right)} \quad (39)$$

The concentration of water is assumed constant, hence is absorbed in the rate coefficient k_1. Note that W_1 is a rate of electron transfer from the cytoplasm to the bio-solution. The following equations complete the bio-electrochemical model:

$$C_{re/rs}\frac{d}{dt}\left(V_{re}-V_{rs}\right)=-A_{re/rs}W_2+\frac{V_{re}-V_{be}}{\mathcal{F}R},$$
$$W_2=k_2\left[\text{e}^-\right]^2_{re}\left[\text{H}^+\right]^2_{rs}\left[\text{O}_2\right]_{rs} \quad (40a)$$

$$\Omega_{rs}\frac{d\text{H}^+_{rs}}{dt}=-2A_{rs/re}W_2+A_{PEM}h_{PEM}\left\{\left[\text{H}^+\right]_{bs}e^{\beta Z_{H^+_{rs}}V_{bs}}-\left[\text{H}^+\right]_{rs}e^{\beta Z_{H^+_{rs}}V_{rs}}\right\} \quad (40b)$$

$$\Omega_{bs}\frac{d\mathrm{H}^{+}_{bs}}{dt} = -A_{PEM}h_{PEM}\left\{\left[\mathrm{H}^{+}\right]_{bs}e^{\beta z_{\mathrm{H}^{+}}V_{bs}} - \left[\mathrm{H}^{+}\right]_{rs}e^{\beta z_{\mathrm{H}^{+}}V_{m}}\right\} + N_{m}A_{bs/m}\widehat{J}_{\mathrm{H}^{+}bs/m} \quad (40c)$$

$$C_{m/bs}\frac{d}{dt}\left[\left(V_m - V_{bs}\right)\right] = A_{m/bs}\mathcal{F}\sum z_i J_{im/bs} \quad (40d)$$

$$C_{be/m}\frac{d}{dt}\left(V_{be} - V_m\right) = -A_{be/m}W_1 \quad (40e)$$

$$C_{re/be}\frac{d}{dt}\left(V_{re} - V_{be}\right) = -A_{re/be}W_1 + \frac{V_{re} - V_{be}}{\mathcal{F}R} \quad (40f)$$

$$C_{bs/rs}\frac{d}{dt}\left(V_{bs} - V_{rs}\right) = \widehat{J}_{\mathrm{H}^{+}bs/rs} \quad (40g)$$

Equations 40e, 40f and 40a describe electron transfer form the bacteria to the anode, from the anode to cathode, and from the cathode to the oxygen in the reference solution. Equation 40g equates the current to charge the membrane between bio- and reference solutions to that part of the proton flux of between these compartments contributing to the boundary layer; this states that at steady-state the current to charge the separating surface is zero, however the proton charge neutral flux is not zero as seen from equation 40b. Equation 40d models the ionic flux between the representative bacterium and bio-solution while equations 40b and 40c follow the temporal evolution of H^+ concentration in the reference solution and bio-solution, respectively.

In the asymptotic limit of zero capacitance the differential equation describing the time course of the potential difference between the two electrodes is well approximated by Ohm's law, an algebraic equation relating the voltage to the electrical current, i.e., $V_{re} - V_{be} = IR$, where I is the current and R is the resistance of the application.

However, this occurs continuously in our formulation when the value of the capacitance in equation 40f is taken to be small. In addition, there may be a voltage difference between the bio-electrode and the bio-solution. However, we assume this potential to be negligible as bacteria cover more 75% of the graphite electrode surface [46]. Hence, the potential difference between the interior of *Geobacter sulfurreducens* and the bio-electrode is equal in magnitude but opposite in sign to the *Geobacter sulfurreducens* membrane potential. Connectivity between the bio-electrode and *Geobacter sulfurreducens* is established by the different electronic transfer modalities mentioned above.

We introduce an additional compartment whose voltage is zero and provides the oxygen needed for the surface reaction producing peroxide in the reference solution. This ground compartment allows us to define the circuit's potential differences since only potential gradients matter as opposed to absolute potentials.

Substrate Storage Granule

The fact that *Geobacter sulfurreducens* can maintain current even when extracellular acetate levels decrease below the detection limit suggests that there is a mechanism by which *Geobacter sulfurreducens* stores acetate or an equivalent substrate internally during times of acetate abundance in the surroundings. The existence of a biochemical storage mechanism is well established for chemotrophic bacteria [47–51] that accumulate massive intracellular stores of sudanophilic granules [52]. These granules consist largely of poly-β-hydroxybyturic acid, $\left(\mathrm{C_4H_6O_2}\right)_\mathrm{n}$ [50]. A biochemical storage mechanism has also been discovered for photosynthetic bacteria. For example, the photosynthetic bacterium *Rhodobacter sphaeroides* stores energy by creating a precipitate particle that is consumed after sunset [53, 54]. This storage mechanism has the advantage that a relatively insoluble particle can maintain a constant (equilibrium) intracellular substrate level over long periods of time until they are dissolved; in contrast, if the

acetate is dissolved in the cytoplasm, it would induce a rapid, short-lived rate of oxidative processing and not be available for later times of starvation. We express this process via an equivalent reversible reaction favoring the production of the stored species. This could explain the consistency in performance of *Geobacter sulfurreducens* in the fuel cell even long after acetate levels in the bio-solution are undetectable. The existence of such a storage mechanism for *Geobacter sulfurreducens* has been suggested [55]. We have assumed cytoplasmic unidirectional inward membrane transport for acetate ions.

Discussion

Computer simulations of the equations of the Materials and Methods section as modified for the fuel cell circuit of Figure 2 are performed. Selected results, together with the specific external conditions are provided in Figures 3-6. The range of electrical currents output by the system, given these external conditions, is consistent with those reported [46]. These results suggest that an electrometabolomics model could be used to optimize microbial fuel cell performance.

Systems consisting of compartments separated by permeable membranes can exhibit complex phenomena arising through the interplay of reaction and transport processes mediated by electrical forces. While strong electrostatic forces constrain the charge density in the interiors of the compartments to zero, oppositely charged layers accumulate on each side of the compartment- defining membranes to create transmembrane potentials that mediate the exchange of ions between compartments. A key element of our theory is the partitioning of the transmembrane flux into a component that charges the layer near the membrane surface, and a charge-neutral one that adds to/subtracts from the bulk within the compartments. As the compartment interiors are charge-neutral, the latter component of the membrane flux must not transport net charge. Our formalism is hierarchical, allowing compartments within compartments as in eukaryotic cells or cell aggregates.

The theory reveals the need to develop charge-conserving reaction networks. In contrast to what is commonly presented in the biochemistry literature, the charges of all molecular species must be given and equations charge balanced. Considering the number of possible states of protonation and other complexing, this is a challenge for self-consistent electrometabolomic modeling. Entropy methods show great promise in the latter regard [56,57]. These methods allow for the calibration of incomplete models using uncertain data.

The generality of our formalism makes it applicable to many microbial systems (e.g., bacteria, eukaryotic cells, tissues) and to subsystems in eukaryotic cells (e.g., mitochondria and the nucleus). The present theory with multiplex bioanalytical experimental techniques will, we believe, enable the modeling of many bioelectric phenomena such as self-organized electro-phoresis [58-60] or patterns of ionic currents that arise in multicellular systems undergoing development or wound healing [13]. With this, we suggest that the present theory holds great promise for attaining quantitative predictions of electrometabolomic phenomena.

The two applications considered in this study illustrate the potential for using electrometabolomic modeling to analyze complex natural and engineered systems. As our simulator is implemented in a hierarchical fashion (i.e. compartments within compartments) it holds great promise for use as an electrometabolomic tissue or organ simulator. This would enable the simulation of developmental phenomena in multicellular systems [13].

Acknowledgments

Special thanks to my wife, my daughters, my intellectual mentor Dr. Peter Ortoleva, and my current mentor Dr. Dennis Daniels.

Reference

1. Garfinkel L et al. 1968. Simulation of the detailed regulation of glycolysis in a heart supernatant preparation. Comput. Biomed. Res. 2(1): 68 – 91.
2. Galazzo JL, Bailey JE. 1990. Fermentation pathway kinetics and metabolic flux control in suspended and immobilized saccharomyces-cerevisiae, Enzyme and Microbial Technology. 12(3): 162 - 172.
3. Cortassa S, Aon MA. 1994. Metabolic control analysis of glycolysis and branching to ethanol production in chemostat cultures of saccharomyces cerevisiae under carbon, nitrogen, or phosphate limitations. Enzyme and Microbial Technology. 16: 761 – 770
4. Bakker BM et al. 1997. Glycolysis in bloodstream form trypanosoma brucei can be understood in terms of the kinetics of the glycolytic enzymes. J. Biol. Chem. 272: 3207 – 3215.
5. Eisenthal R, Cornish-Bowden A. 1998. Prospects for antiparasitic drugs: the case of trypanosoma brucei, the causative agent of african sleeping sickness. J. Biol. Chem.. 273: 5500 – 5505.
6. Bakker BM et al. 2000. Compartmentation protects trypanosomes from the dangerous design of glycolysis. Proc. Natl Acad. Sci. USA. 97: 2087 – 2092.
7. Teusink B et al. 2000. Can yeast glycolysis be understood in terms of in vitro kinetics of the constituent enzymes? Testing Biochemistry. Eur. J. Biochem. 267: 1 – 18.
8. Zamamiri AM, Birol G, Hjortsø MA. 2001. Multiple stable states and hysterisis in continuous, oscillating cultures of budding yeast. Biotech. Bioeng. 73: 305 – 312.
9. Baier G, Muller M, Ørsnes H. 2002. Excitable spatio-temporal chaos in a model of glycolysis. J. Phys.Chem. 106: 3275 – 3282.
10. Navid A, Ortoleva PJ. 2004. Simulated complex dynamics of glycolysis in the protozoan parasite trypanosoma brucei. J. Theor. Biol. 228: 449 – 458.
11. Weitzke EL, Ortoleva PJ. 2003. Simulating cellular dynamics through a coupled transcription, translation, metabolic model, Comp. Bio. and Chem. 27: 469 -481.
12. Jaffe LF: Control of development by ionic currents. In Membrane Transduction Mechanisms. Edited by Cone RA and Dowling JE. New York: Raven Press; 1979: Soc. Gen. Physiol. Ser. 33
13. Ortoleva PJ: Developmental bioelectricity. In Biological Effects of Nonionizing Radiation. Edited by Illinger KH. Washington: American Chemical Society; 1981: 163 - 212. .
14. London RE, Gabel SA. 1989. Determination of membrane potential and cell volume by 19F NMR using trifluoroacetate and trifluoroacetamide probes. Biochemistry. 28: 2378 – 2382.
15. Adebodun F, Post JFM. 1993. 19F NMR studies of changes in membrane potential and intracellular volume during dexamethasone-induced apoptosis in human leukemic cell lines. J. Cell Physiol. 154: 199 – 206.
16. Miller PGG. 1984. Alternate pathways in protozoan energy metabolism. Parasitology. 82: 23 – 25.
17. Nolan PD, Voorheis HP. 2000. Factors that determine the plasma-membrane potential in bloodstream forms of Ttrypanosoma brucei. Eur. J. Biochem. 267: 4615 – 4623.
18. Courtemanche M et al. 1998. Ionic mechanisms underlying human atrial action potential properties: insights from a mathematical model. American J Physiol. 275: H301 – H321.
19. Virgilio L, Bookchin RM. 1986. Volume, pH, and ion-content regulation in human red cells: analysis of transient behavior with an integrated model. J. Memb. Biol. 92: 57 – 74.
20. Hille B: Ion Channels of Excitable Membranes. Third Edition. Massachusetts: Sinauer Associates, Inc. 2001.
21. Saimi Y et al. 1992. Patch clamp studies on microbial ion channels. Methods in Enzymology. 207: 681 – 691.
22. Bashford CL, Pasternak CA. 1985. Plasma membrane potential of neutrophils generated by the Na+-pump. Biochem. Biophys. Acta 817: 174 – 180.
23. Inoue II et al. 2002. Ionic currents in isolated and in situ squid schwann cells. J. of Physiol. 541 (pt 3): 769 – 778.
24. Poberaj I et al. 2002. Modeling excess retrieval in rat melanotroph membrane capacitance records. Biophysical Journal. 82 (pt 1): 226 – 232.
25. Olschewski A et al. 2002. Graded response of K+ current, membrane potential, and [Ca2+]I to hypoxia in pulmonary arterial smooth muscle. American Journal of Physiology – Lung Cellular & Molecular Physiology. 283(5): 1143 – 1150.
26. Leppanen L, Stys PK. 1997. Ion transport and membrane potential in CNS myelinated axons II. Effects of metabolic inhibition. J. of Neurophysiology 78: 2095 – 2107.
27. Oghalai JS et al. 2000. Voltage- and tension-dependent lipid mobility in the outer hair cell membrane. Science. 287: 658 – 661.
28. Yasui K et al. 2001. If current and spontaneous activity in mouse embryonic ventricular myocytes. Circ Res. 88: 536 – 542.
29. Terasawa K.et al. 2002. Nonselective cation currents regulate membrane potential of rabbit coronary arterial cell. Circulation. 106: 3111 – 3119.
30. Bernstein J. 1902. Untersuchungen Zur Thermodynamik der Bioelectrichen Strome. Pfluegers Arch. 92: 521 – 562.
31. Berstein J: Elektrobiologie. Braunschweig: Vieweg F; 1912.
32. Goldman DE. 1943. Potential, impedance, and rectification in membranes. J. Gen. Physiol. 27: 37 – 60.
33. Hodgkin A, Huxley AA. 1952. Quantitative description of membrane current and its application to conduction and excitation in nerve. J. Physiol. 117: 500 – 544.
34. http://en.wikipedia.org/wiki/Hodgkin-huxley_model
35. Fontus MWA: Simulating the Electrometabolome, Ph. D. Thesis, Indiana University, 2007.
36. Renard F et al. 1998. Experimental evidence for self-organization during reactive fluid flow in a porous medium. Geophysical Research Letters. 25: 385 – 388.
37. Opperdoes FR. 1987. Compartmentation of carbohydrates metabolism in trypanosomes. Annual Review Microbiology. 41: 127 – 151.
38. Brown PN, Byrne GD, Hindmarsh AC. 1989. VODE: A Variable coefficient ODE solver. SIAM J. Sci. Stat. Comput. 10: 1038-1051.
39. Byrne GD, Hindmarsh AC. 1975. A polyalgorithm for the numerical solution of ordinary differential equations ACM Trans. Math. Software. 1: 71 - 96.
40. Hindmarsh AC, Byrne GD. 1977. EPISODE: an effective package for the integration of systems of ordinary differential equations. LLNL Report UCID/30112, Rev. 1.
41. Byrne GD, Hindmarsh, A. C. EPISODEB: An Experimental Package for the Integration of Systems of Ordinary Differential Equations with Banded Jacobians. LLNL Report UCID/30132, April 1976.
42. Hindmarsh AC: ODEPACK, a systematized collection of ODE solvers. In Scientific Computing, Edited by Stepleman RS et al.

Amsterdam: (Vol. 1 IMACS Transactions on Scientific Computation); 1983: 55 - 64.
43. Jackson KR, Sacks-Davis R. 1980. An alternative implementation of variable step-size multistep formulas for stiff ODEs. ACM Trans. Math. Software. 6: 295 - 318.
44. Logan BE et al. 2006. Microbial fuel cells: methodology and technology. Env. Sci. & Technol. 40: 5181 – 5192.
45. Bond DR et al. 2002. Electron-reducing microorganisms harvesting energy from sediments. Science. 295: 483 – 485.
46. Bond RD, Lovley DR. 2000. Electricity production by *geobacter sulfurreducens* attached to electrodes. Appl. Environ. Microbiol. 69: 1548 – 1555.
47. Forsyth WGC et al. 1958. Occurrence of poly-β-hydroxybutyric acid in aerobic gram-negative bacteria. Nature. 182: 800 – 801
48. Doodoroff M, Stanier RY. 1959. Role of poly-β-hydroxybutyric acid in aerobic gram-negative bacteria. Nature. 183: 1440 – 1442.
49. Lemoigne M. 1927.Etudes sur l'autolyse microbienne. Origine de l'ccide β-oxybutyric forme par autolyse. Ann. Inst. Pasteur. 41: 148 – 166.
50. Lemoigne M, Girard H. 1943. Reserves lipidiques β-hydroxybutyriques chez *azobacter chroococcum*. Compt. Rend. Acad. Sci. Paris. 217: 557 – 558.
51. Morris MB, Roberts JB. 1959. A group of pseudomonads able to synthesize poly-β-hydroxybutyric acid. Nature. 183: 1538 – 1539.
52. Reguera G et al. 2006. Biofilm and nanowire production lead to increased current production in microbial fuel cell. Appl. Environ. Microbial. 72: 7345 – 7348.
53. Stanier RY. 1961. Photosynthetic mechanism in bacteria and plants: development of a unitary concept. Bacteriol. Rev. 25: 1 – 17.
54. Tavano CL, Donahue TJ. 2006. Development of the bacterial photosynthetic apparatus. Curr. Opin. Microbiol. 9(6): 625 – 631.
55. Freguia S et al. 2007. Electron and carbon balances in microbial fuel cells reveal temporal bacterial storage behavior during electricity generation. Environ. Sci. Technol. 41(8): 2915 – 2921.
56. Sayyed-Ahmad A, Tuncay K, Ortoleva PJ. 2003. Toward automated cell model development through information theory. J. Phys. Chem. A. 107 (49): 10554 - 10565.
57. Sayyed-Ahmad A, Tuncay K, Ortoleva PJ. 2007. Transcriptional regulatory network refinement and quantification through kinetic modeling, gene expression microarray data and information theory. BMC Bioinformatics. 8:20, doi: 10.1186/1471-2105-8-20.
58. Later R, Ortoleva PJ. 1982. A study of instability to electrical symmetry breaking in unicellular systems. J. Theor. Biol. 96:175 - 200.
59. Larter R, Ortoleva PJ. 1981. A theoretical basis for self-electrophoresis. J. Theor. Biol,. 88: 599 - 630.
60. Cord-Ruwisch R et al. 1998. Growth of *g. sulfurreducens* with acetate in syntrophic coorperation with hydrogen-oxidizing anaerobic partners. Appl. Environ. Microbiol. 64: 2232 – 2236.
61. Damper PD, Epstein W. 1981. Role of the membrane potential in bacterial resistance to aminoglycoside antibiotics. Antimicrobial Agents and Chemotherapy. 20(6): 803 - 808.